Around the Ising Model

Fernando Mora, Felipe Urbina, Vasco Cortez, and Sergio Rica

Abstract This article discuss several features and connections arising in a class of Ising-based models, namely the Glauber-Ising time dependent model, the Q2R cellular automata, the Schelling model for social segregation, the decision-choice model for social sciences and economics and finally the bootstrap percolation model for diseases dissemination. Although all these models share common elements, like discrete networks and boolean variables, and more important the existence of an Ising-like transition; there is also an important difference given by their particular evolution rules. As a result, the above implies the fact that macroscopic variables like energy and magnetization will show a dependence on the particular model chosen. To summarize, we will discuss and compare the time dynamics for these variables, exploring whether they are conserved, strictly decreasing (or increasing) or fluctuating around a macroscopic equilibrium regime.

Fernando Mora
Facultad de Ingeniería y Ciencias, Universidad Adolfo Ibáñez, Avda. Diagonal las Torres 2640, Peñalolén, Santiago, Chile, e-mail: femora@alumnos.uai.cl

Felipe Urbina
Facultad de Ingeniería y Ciencias, Universidad Adolfo Ibáñez, Avda. Diagonal las Torres 2640, Peñalolén, Santiago, Chile, e-mail: felipe.urbina@uai.cl

Vasco Cortez
Facultad de Ingeniería y Ciencias, Universidad Adolfo Ibáñez, Avda. Diagonal las Torres 2640, Peñalolén, Santiago, Chile, e-mail: vcortez@alumnos.uai.cl

Sergio Rica
Facultad de Ingeniería y Ciencias, Universidad Adolfo Ibáñez, Avda. Diagonal las Torres 2640, Peñalolén, Santiago, Chile, e-mail: sergio.rica@uai.cl

1 Introduction

The Ising model, introduced in the early 1920's, by Lenz [1] and Ising [2] as a thermodynamical model for describing ferromagnetic transitions has evolved as one of the most prolific theories in the twenty century opening a huge number of new areas of knowledge (For an historical review see [3]). The importance of the Ising model raises in its universality and robustness, indeed despite its simplicity, this model has been the starting point for the emergence of various subfields in physical (and social) sciences, namely, phase transitions, renormalisation group theory, spin-glasses, lattice field theories, etc.

In the current contribution, we shall discuss four distinct applications of Ising-based models with applications to both statistical mechanics as social sciences. The first one is devoted to the Glauber-Ising time dependent model with applications to decision-choice theory in economics and social sciences. In the sixties Glauber [4], introduced an stochastic time dependent rule to mimic the statistical properties of the original Ising problem. Glauber's dynamics has been considered in the context of social sciences by Brock and Durlauf [5, 6], and, more recently, by Bouchaud [7].

The second topic is Q2R automata model introduced in the 80s by Vichniac [8]. The Q2R[1] possess time reversal symmetry, which is at the core of any fundamental theory in physics. Moreover, the temporal evolution of this automata conserves a quantity which is closely related to the energy of the Ising model [9]. We are interested in this model because is a natural starting point for studying the statistical and typical irreversible behavior of reversible systems. As shown in Ref. [10], this system evolves in an irreversible manner in time towards an "statistical attractor", moreover the macroscopic observable, the so called global magnetization, depends on the value of the initial energy following a law which is exactly the one obtained theoretically by Onsager [11] and Yang [12], more than 60 years ago. Moreover, in Ref. [13] it is shown how this model exhibits the same features of Hamiltonian systems with many degrees of freedom, that is, a sensibility to initial conditions, positive Lyapunov exponents, among others.

The third model that we shall discuss in this article concerns the Schelling model of social segregation, introduced in the early seventies by Thomas C. Schelling [14, 15, 16]. This model became one of the paradigm of an individual-based model in social science. Schelling's main contribution is that shows on the formation of a large scale pattern of segregation as a consequence of purely microscopic rules. More recently, it has been shown that the Ising energy, which is a good measure of segregation, acts as a Lyapunov potential of the system is driven, under particular conditions, by a strictly decreasing energy principle [17].

Finally, we shall discuss a model for dissemination's disease known as Bootstrap percolation, first introduced in the late seventies by Chalupa, Leath and Reich [18]. In this model a healthy individual may be infected if the majority of its neighbors are infected. On the other hand an infected individual never recovers, so it remains

[1] Q by four, *quatre*, in french, 2 by two steps automata rule as explicitly written below, and R by reversible.

infected forever. This model has been used as a model for disease's propagation. One of the most important questions arising is the determination of the critical number of infected individuals to contamine the whole population.

The paper is organized as follows, in section 2, some common features, as well as, the precise rules for each particular model are explicitly described. Next, in section 3 the main dynamical behavior, the salient properties and the phase transitions are shown and explained, for each of them. Finally, we conclude.

2 Ising-based models

2.1 Generalities

2.1.1 The lattice and the neighborhood

All models discussed below, display similar features, the system consisting of a lattice with $N \gg 1$ nodes, in which each node, k, may take a binary value $S_k(t) = \pm 1$ at a given time. Each node k on the lattice interacts, in general, with all other individuals, with an interaction coefficient J_{ik} (i denotes an arbitrary node). But in particular, a node, k, may interact only with a finite neighborhood denoted by V_k. The number of neighbors for site k, $|V_k|$, is the total number of non zero J_{ik} for each node. In Fig. 1 we show, as an example, four possible lattice configurations.

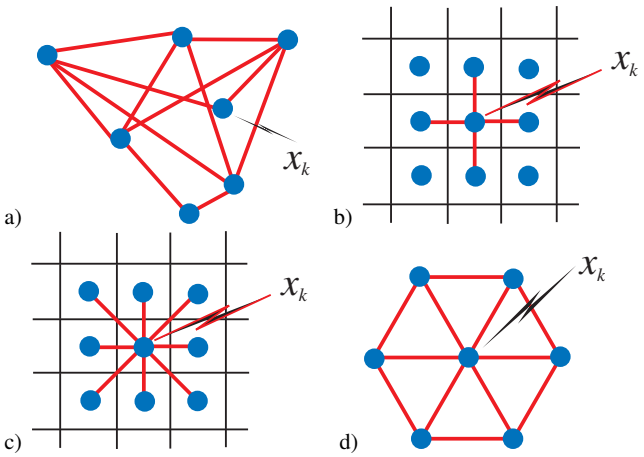

Fig. 1 Examples of lattices and neighborhoods. We illustrate explicitly: a) an arbitrary network with a random number of neighborhoods; and three periodic regular lattices in two space dimensions: b) a square lattice with a von-Neuman neighborhood of 4 individuals (the original lattice of the Ising model with the nearest neighborhood); *c)*, a square lattice with a Moore neighborhood of 8 individuals, and d) a hexagonal lattice with 6 neighborhoods.

2.1.2 The "energy" and the "magnetization".

We define the macroscopic observables of the system, by analogy with the original Ising model of ferromagnetism, as follows:

$$E[\{S\}] = -\frac{1}{2}\sum_{i,k} J_{ik} S_i(t) S_k(t)\,, \tag{1}$$

$$M[\{S\}] = \sum_{k=1}^{N} S_k(t)\,. \tag{2}$$

These quantities will be the pertinent observables, and we shall use them to classify the distinct cases that we will be described in the next sections.

2.2 The time-dependent Glauber-Ising Model

Glauber [4], in the sixties, introduced a dynamical model for the study of the Ising model. The rule governing Glauber's model is the following:

Let, the local magnetization at the site k and at a time t, be:

$$U_k(t) = B + \sum_i J_{ik} S_i(t), \tag{3}$$

with B being an external magnetic field. Then, the spin's value at the next time step, $t+1$, will be

$$S_k(t+1) = \mathrm{sgn}(U_k(t)), \tag{4}$$

that is $S_k(t+1) = +1$ if $U_k(t) \geq 0$ and $S_k(t+1) = -1$ if $U_k(t) < 0$. We call (4) the deterministic rule. In probability language, if $U_k(t) \geq 0$, then $S_k(t+1)$ would be +1 with probability 1, and it would be -1 with probability 0. This rule is updated in parallel fashion.

Next, this deterministic rule may be modified by a probabilistic rule, in the following way:

$$S_k(t+1) = \begin{cases} +1 & \text{with probability} \quad p = \frac{1}{1+e^{-\beta U_k(t)}} \\ -1 & \text{with probability} \quad p = \frac{1}{1+e^{\beta U_k(t)}} \end{cases} \tag{5}$$

Notice that in the limit $\beta \to \infty$ one recovers the deterministic behavior (4), while in the limit $\beta \to 0$ one reaches a completely random (binomial) dynamics regardless of the value of U, that is $S_k(t+1)$ would be +1 with probability 1/2.

The Glauber rule is indeed a Markov chain which manifests, in a perfect way, the statistical properties of the Ising phase transition for the case of Von-Neuman neighbourhoods, and it also agrees with the mean field approximation for the case of a large number of neighbours . Finally, nowadays the Glauber dynamics is the starting point for numerical simulations of spin glasses systems with random values for the J_{ik} coefficients.

2.2.1 Random Decision-Choice Model

Let us consider now a random choice model [5, 6, 7] in the context of social sciences. An individual takes a choice based on a combination of decision quantities, namely an individual "decision parameter" f_k, a "global decision" or "public information" parameter $F(t)$ (which could be included in the previous individual decision parameter) and a "social pressure" $\sum_i J_{ik}S_i(t)$.

Next take[2], $U_k(t) = f_k + F(t) + \sum_i J_{ik}S_i(t)$, and follow the Glauber deterministic dynamics (4) or more generally the Glauber random dynamics (5).

Due to both, the Ising-like feature as the Glauber Dynamics evolution rule, a phase transition is known to appear. This transition favors the decision into one or another of the two options of the binary variable.

2.3 The Q2R automata

The Q2R rule considers the following two-step rule which is updated in parallel [8] [3]:

$$S_k(t+1) = S_k(t-1) \times \begin{cases} +1 & \text{if} \quad \sum_i J_{ik}S_i(t) \neq 0 \\ -1 & \text{if} \quad \sum_i J_{ik}S_i(t) = 0 \end{cases} \tag{6}$$

Naturally, it is possible to add, without any difficulty, an external magnetic field B. However, some caution should be taken into account: the model works if $U_k(t) = B + \sum_i J_{ik}S_i(t)$, may vanish, therefore, B and the J_{ik} factors should be integers. For instance in the case of a finite neighborhood, $B + |V_k|$ should be an even number.

The rule (6) is explicitly invariant under a time reversal transformation $t+1 \leftrightarrow t-1$. Moreover, as shown by Pomeau [9], the following quantity, that we may call an energy, despite not being exactly the energy (1)

[2] The so called "perceive overall incentive agent function", by Bouchaud [7].

[3] This two-step rule may be naturally re-written as a one-step rule with the aid of an auxiliary dynamical variable [9].

$$E[\{S(t),S(t-1)\}] = -\frac{1}{2}\sum_{i,k} J_{ik}S_k(t)S_i(t-1), \tag{7}$$

is preserved under the dynamics defined by the Q2R rule (6). Moreover, the energy is bounded by $-2N \leq E \leq 2N$.

The rule (6) is complemented with an initial condition $S_k(t=0)$ and $S_k(t=1)$ that will be described more precisely in the next section.

2.4 Schelling model for Social segregation.

Schelling model, is also characterized by a binary variable S_k which may take values +1 and -1. We shall say that an individual S_k at the node k is "happy" at his site, if and only if, there are less than θ_k neighbors at an opposite state. θ_k is a tolerance parameter that depends in principle on the node and, it may take all possibles integer values, such that $0 < \theta_k < |V_k|$ (we exclude the cases $\theta_k = 0$ and $\theta_k = |V_k|$ from our analysis). The satisfaction criterion reads[4]

An individual S_k is unhappy at the node k *if and only if*:

$$\sum_{i\in V_k} S_i = \begin{cases} |V_k| - 2n_k(-1) \leq |V_k| - 2\theta_k, \text{ if } S_k = +1 \\ 2n_k(-1) - |V_k| \geq 2\theta_k - |V_k|, \text{ if } S_k = -1. \end{cases} \tag{8}$$

Here $n_k(+1)$ is the number of neighbors of S_k that are in the state $+1$; and, $n_k(-1)$ the number of neighbors of S_k in the state -1, naturally $n_k(+1)+n_k(-1) = |V_k|$.

Having labeled all different un-happy individuals, one takes randomly two of them in opposite states (one +1, and one -1) and exchanges them. Even when this is not exactly the original Schelling's rule, the present *Schelling's protocol* is a simpler one. In any case, it can be modified in a straightforward way to include for example vacancies [19, 20], different probabilities of exchange [19], multiple states variables [21], etc.

If k and l are these random nodes, then the evolution rules:

[4] The criteria (8) may be unified in a single criteria [17] (multiplying both sides of the two inequalities by S_k):

$$\text{an individual } S_k \text{ is unhappy at the node } k \text{ if , and only if, } S_k \sum_{i\in V_k} S_i \leq |V_k| - 2\theta_k,$$

which is a kind of energy density instead of the threshold criteria found in Glauber dynamics (4).

$$S_k(t) \to S_k(t+1) = -S_k(t), \quad S_l(t) \to S_l(t+1) = -S_l(t)$$

and for all other nodes $i \neq k \,\&\, l$ remain unchanged $S_i(t) \to S_i(t+1) = S_i(t)$.

The protocol is iterated in time forever or until the instant when one state does not have any unhappy individuals to be exchanged.

Notice, that Schelling criteria (8) is deterministic, however the exchange is a random process, therefore two initial configurations will not display the same behavior in detail, but they will evolve to the same statistical attractor [22].

Schelling's protocol, defined above, has a remarkable property: if $\theta_k > \frac{|V_k|}{2}$ then any exchange $k \leftrightarrow l$, will always decrease the energy

$$E[\{S\}] = -\frac{1}{2}\sum_k \sum_{i \in V_k} S_i(t) S_k(t). \tag{9}$$

The energy (9) follows from (1), whenever $J_{ik} = 1$ for neighbors and $J_{ik} = 0$ otherwise.

For a proof, we refer to Ref. [17]. We shall only add the following remark: if $\theta_k > \frac{|V_k|}{2}$, then the evolution necessarily stops in finite time. This is because the energy (9) is bounded from below by $E_0 = -\frac{1}{2}\sum_{k=1}^{N} |V_k|$ and because the energy (1) decreases strictly. On the other hand, for $\theta_k < \frac{|V_k|}{2}$, the energy may increase or decrease after an exchange indistinctly.

2.5 Bootstrap percolation

We shall consider the problem of bootstrap percolation for a given lattice [18]. As in the previous models, each node k interacts with $|V_k|$ neighbors, the neighborhood defined by the set V_k. As before the state, S_k may take values +1 and -1 depending on if it is "infected" or not. At a given "time" the state $S_k(t)$ evolves into $S_k(t+1)$ under the following parallel rule: if a site is not infected, and if the *majority* of its neighbors are infected, then the site becomes infected [23]. On the other hand, if the site is already infected it keeps its infected state.

Summarizing, the evolution rule, which is updated in parallel, may be written in the following general way:

$$\text{if } S_k(t) = -1 \text{ and } \sum_k S_k(t) > 0, \text{then } S_k(t+1) = +1, \tag{10}$$

otherwise, if $S_k(t) = 1$ then $S_k(t+1) = 1$.

From the dynamics it follows directly that the energy (9) decreases in time, $E(t+1) \leq E(t)$, as well as the magnetization increases in time: $M(t+1) \geq M(t)$. As in the case of the Schelling model, because the energy is a strictly decreasing functional, and because it is bounded from below in a finite network, then the dynamics always stops in finite time.

Finally, let us comment that a problem that has increased in interest in recent times deals with the question of how the total infection depends on the initial configuration which is randomly distributed and such that a site will be at the state $S_k = +1$ with a probability p [24].

Naturally, if initially $p \approx 1/2$, then every site has in average the same number of $S_k = +1$ states and $S_k = -1$ in its neighborhood, then the system would percolate almost in one step. However, as p decreases, one can define a probability, $P(p)$, which is the probability that the system would percolate at the end of the evolution process. At the end this probability can be numerically determined.

2.6 Recapitulation

The afore mentioned models have in common a threshold criteria (4), (6), (8), and (10) the subsequent dynamics follows different rules. Therefore one should expect distinct properties.

The Glauber Dynamics does not preserve neither the energy or magnetization, however the Q2R dynamics (Sec. 2.3) does preserve only the energy but does not preserve the magnetization. The Schelling model (Sec. 2.4) does preserve only the magnetization, but if $\theta_k > |V_k|/2$ the system's energy is strictly a decreasing function. Finally, in the infection model of section 2.5, the energy strictly decreases whereas the magnetization is an increasing function of time.

Table 1 Recapitulation of the four above mentioned models, and its main conservation properties.

Dynamics	Evolution Criteria	Energy	Magnetisation
Glauber	$\mathrm{sgn}(B+\sum_i J_{ik}S_i(t))$	Not Conserved	Not Conserved
Q2R	$\sum_i J_{ik}S_i(t)) = 0$	Conserved	Not Conserved
Schelling	$\mathrm{sgn}(S_k(t))\sum_{i\in V_k} S_i(t) \leq \lvert V_k\rvert - 2\theta_k$	Not Conserved [a]	Conserved
Bootstrap	$\sum_{i\in V_k} S_i(t) > 0$	$\Delta E < 0$	$\Delta M > 0$

[a] If $\theta_k > |V_k|/2$ then $\Delta E < 0$.

3 Ising patterns, transitions, and dynamical behavior

In this section, we shall roughly describe the essential phenomenology of the Ising-like models and rules described in the previous section, whether they are governed (or not) by the rules of conservation of magnetization energy.

3.1 Glauber and Decision-Choice model dynamics

The time dependent Glauber-Ising model shows a very rich phenomenology. As such, the model's behavior has been explored using mean field approximation (the Curie-Weiss law) as well as by direct simulations of the rule (5). Here our macroscopic observable is the total magnetization per site, namely $M(t)/N$ and were $M(t)$ is defined in equation (2). In what it follows, we will only show results for the direct simulation of the Glauber-Ising model (4) and we shall use the terminology of social sciences [7]. In Figure 2 we show three distinct states characterized by different values of the parameter of "irrationality" β,[5] and a null value for the public information parameter $F(t)$.

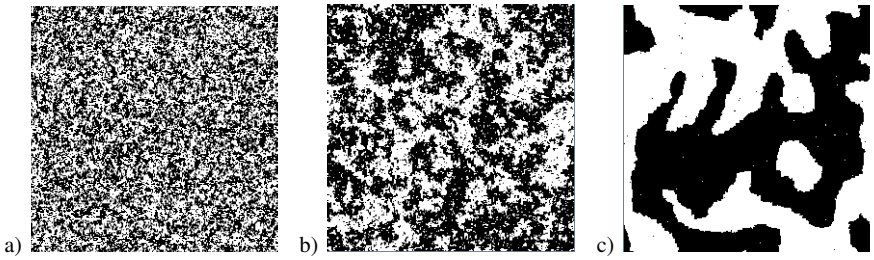

Fig. 2 Snapshots of the patterns for the Glauber-Ising model. The simulation is for a $N = 256 \times 256$ periodic lattice with von Neuman neighborhood. Moreover we take $f_k = 0$ and $F = 0$. The parameter of "irrationality" and the magnetization averages are, respectively : a) corresponds to a paramagnetic phase for $\beta = 0.53$ and $\langle M \rangle / N = 0.0006$; b) a critical phase for $\beta = 0.82$ and $\langle M \rangle / N = 0.02$; and c) corresponds to a ferromagnetic phase $\beta = 1.8$, and $\langle M \rangle / N = 0.39$.

In Fig. 3 we show two different figures for the mean magnetization $\langle M \rangle / N$ versus the irrationality parameter β, divided into two groups depending on the non-zero or null value for the public information parameter $F(t)$. Each point, was calculated for a total of approximately 2×10^4 time steps. We can readily observe the appearance of a bifurcation for the case $F = 0$ and β greater than $\beta_c = 0.8$

Therefore, the time dependent Glauber-Ising model displays a transition from a paramagnetic to a ferromagnetic phase for $\beta_c \approx 0.8$ which is in agreement with the critical threshold value of the Ising model, $\beta_c = \log(1+\sqrt{2}) \approx 0.881\ldots$

[5] In statistical physics, β is the inverse of the thermodynamical temperature, $\beta \sim 1/T$.

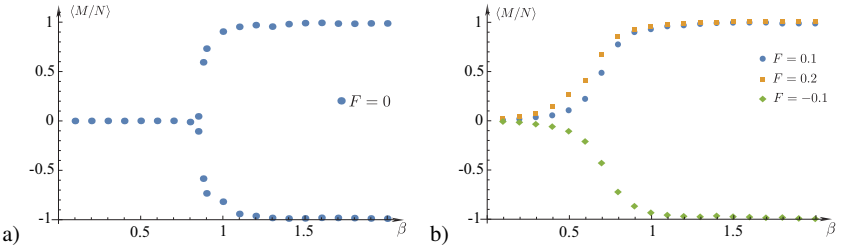

Fig. 3 Average magnetization $\langle M \rangle$ versus β. The average are taken from long time simulations of approximately 20000 time steps. In both cases the random external field is settled to zero $f_k = 0$. a) Case of $F = 0$; and , b) Cases of $F = \pm 0.1$ and $F = 0.2$.

3.2 Q2R dynamics

We shall now present the dynamics of the Q2R model for the case of von Neuman vicinity (the coupling interaction $J_{ik} = 1$ for the four closest neighbors), which is the original Q2R cellular automata [8].

The time evolution of magnetization, given an initial energy value E/N, provides a direct observation of the spin's dynamics and fluctuations. In what it follows, we will base our results and analysis taking a periodic grid of size $N = 256 \times 256$.

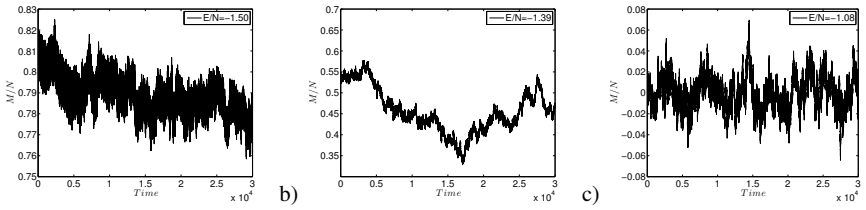

Fig. 4 Three types of magnetization dynamics for a running time of $T = 3 \times 10^4$ time steps, and considering three different values of energy. Figure a) corresponds to an initial energy $E/N = -1.50$, figure b) corresponds to an initial energy $E/N = -1.39$ and figure c) corresponds to an initial energy $E/N = -1.08$. The three figures show the fluctuations in the macroscopic observable $M(t)$.

When the initial energy value is $E/N = -1.50$, which refers to figure $4(a)$, it can be seen that the system's dynamics fluctuates without significative changes in the magnetization's value. This means that the overall set of spins are oriented in a preferred direction. This is known as a ferromagnetic state. If we raise the initial energy value and take $E/N = -1.39$, which corresponds to figure $4(b)$, the dynamics abruptly fluctuates because of the closeness to the critical energy value: E_c/N [10]. Finally, if the initial value of the energy is greater than in the previous cases, *e.g* $E/N = -1.08$, figure $4(c)$ shows how the dynamics of magnetization decays reaching a zero mean value $\langle M \rangle \approx 0$.

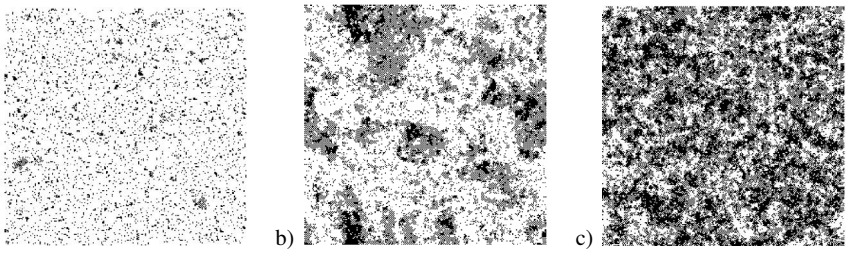

Fig. 5 Snapshots of spin structure at $T = 3.5 \times 10^4$ considering three initial values. Figure a) corresponds to an initial energy $E/N = -1.50$ and a magnetization $M/N = 0.79$, figure b) corresponds to an initial energy $E/N = -1.39$ (which is close to the transition energy $E/N = \sqrt{2}$) and $M/N = 0.455$; and, figure c) corresponds to an initial energy $E/N = -1.08$ and c) $M/N = 0.012$.

Similarly, figure 5 shows some characteristic snapshots of the spin field patterns at a given time for the same energy per site. When the energy value is $E/N = -1.50$ (see Fig. 5-a), it can be seen how the spins are organized with a well defined magnetization, namely $S_k = +1$ or $S_k = -1$. This is a ferromagnetic phase. However, when the initial energy value is $E/N = -1.39$ (close to the critical energy), as shown in figure 5-b, the system generates patterns characterized by well defined clusters of states. Finally, for an energy $E/N = -1.08$ (see figure 5-c) the system shows an homogeneous state with the spin distributed more or less randomly, which characterizes a paramagnetic phase.

Also it can be shown that the average magnetization $\langle M \rangle$ depends critically on the initial energy, E/N, of the system[6].

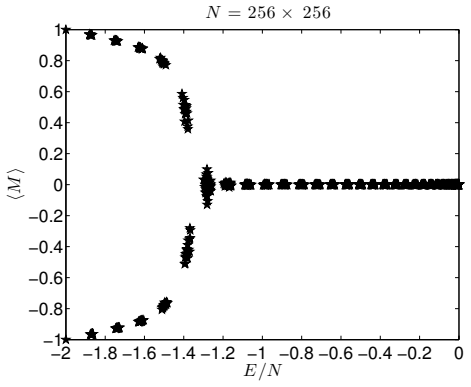

Fig. 6 Phase transition diagram for the average Magnetization $\langle M \rangle$ versus initial energy E/N, for a grid size $N = 256 \times 256$.

Finally, we can state three fundamental features from the above phase diagram. First, there exists a zone in which the system stays into a ferromagnetic state when

[6] Q2R is a micro canonical description of the Ising transition, therefore we use the energy in absence of any temperature. In Ref. [10] it is shown the excellent agreement among the Q2R bifurcation diagram with the Ising thermodynamical transition.

the value of the energy is lower than the critical energy $E < E_c$. Secondly, there is a second order phase transition at $E_c/N = -\sqrt{2}$ and it is formally equivalent to the Ising critical temperature [10]. Third, when the initial energy value is greater than the critical energy $E > E_c$, the system presents a paramagnetic phase, with a magnetization value $\langle M \rangle = 0$.

3.3 Schelling dynamics

We shall characterize the dynamics of Schelling model for the particular case in which the system is a two dimensional periodic lattice, and each site possess the same neighborhood consisting in the $|V|$ closest individuals. We shall consider also that the parameter θ_k is uniform, that is, $\theta_k = \theta$.

Fig. 7 displays an example of typical patterns arising in the Schelling's model. As it can be observed, the dynamics depends critically on the value of the tolerance parameter θ, defined above. More precisely, if θ is larger or smaller than $\theta_{c_1} = |V|/4$, $\theta_c = |V|/2$, and $\theta_{c_2} = 3|V|/4$. The initial state was chosen randomly with a binomial distribution, that is $S_k(t=0)$ was +1 with probability 1/2 and -1 with the same probability. Hence, the total magnetization is $M(t=0) \approx 0$, and it is kept fixed during the evolution.

The simulation shown in Fig. 7, corresponds to a Schelling rule with a vicinity of $|V| = 20$ elements. Clearly three different cases can be distinguished, and at least three transition points, namely $\theta_{c_1} = |V|/4$, $\theta_c = |V|/2$, and $\theta_{c_2} = 3|V|/4$. For $1 < \theta \leq |V|/4$ (see Fig. 7-a) one observes a non-segregated pattern, the states $S_k = \pm 1$ are swapping, more or less randomly in the system, without a formation of any kind of large scale structure. In a coarse graining scale, for instance, the scale of the vicinity, the coarse-grained magnetization, namely, $m = \frac{1}{|V|}\sum_{i \in V_k} S_i(t)$ is zero everywhere, as well as the energy[7]. In this situation, it is tempting to make an analogy with the Ising paramagnetic phase. For $|V|/4 < \theta \leq |V|/2$, one observes how a segregation pattern arises (see Fig. 7-b & c). More important the coarse-grained magnetization is locally non-zero, and the pattern presents domain walls, which are characteristic of a ferromagnetic phase in the Ising-like terminology. For $|V|/2 < \theta \leq 3|V|/4$, one observes also segregation (see Fig. 7-e), but the dynamics stops in a finite time. The final state is a quenched disordered phase for which one may conjecture an analogy with a "spin glass" phase, and the appearance of a kind of long-range order. The case $\theta = 3|V|/4$ in (see Fig. 7-f) it is interesting because, although the are some islands of segregation, the system also recovers its original heterogeneity, with almost a null coarse-grained magnetization m.

[7] Notice that, as already said, the total magnetization is constant in the Schelling model. Therefore we cannot match the Schelling transitions observed here with the phase transition for the cases of the Glauber-Ising and the Q2R models.

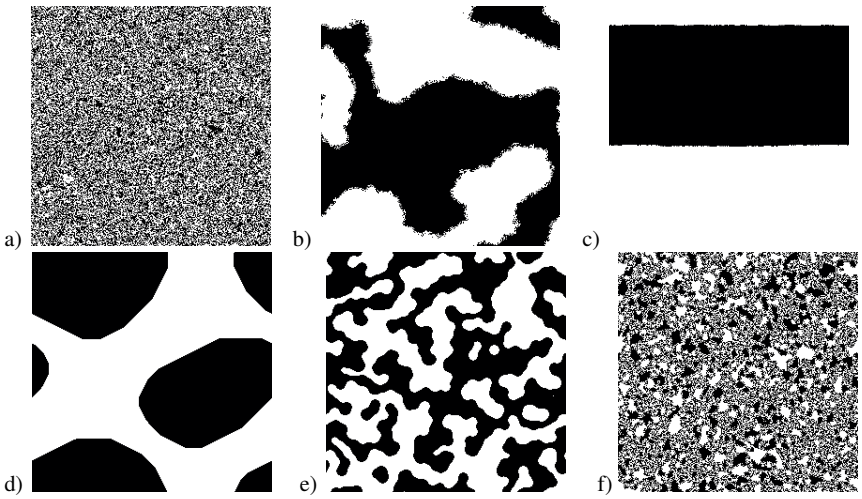

Fig. 7 Schelling's patterns for various satisfaction parameter θ in a square periodic lattice of $N = 256$ nodes. The vicinity is uniform and contains $|V| = 20$ elements. a) $\theta = 5$; b) $\theta = 6$; c) $\theta = 9$; d) $\theta = 10$ (eventually this case the two spots observed merges into a single one, this coalescence dynamics, however, it happens after a longtime); e) $\theta = 11$ and f) $\theta = 15$, are two cases whenever the energy is a strictly decreasing function so the dynamics stops in finite time, in the former case this happens after a time so segregation is possible, however in the later case the dynamics stops shortly after the Schelling algorithm started. For $\theta = 15$ we say that this is a frustrated dynamics, because the system cannot reach the ground state energy because the dynamics stops after one of the population is completely happy.

3.4 Bootstrap percolation

The spin dynamics for the case of Bootstrap percolation of Section 2.5 is always characterized by an energy decreasing principle, moreover because a +1 spin never flips to a -1, the magnetization is mandated to increase up to a constant value because of the impossibility to infect more individuals, or simply because the system has been fully percolated by the +1 spin states.

As said in Sec. 2.5, we shall consider a random initial state with a fraction p of the spins at the state $S_k = +1$ (that is, a fraction p of the population would be infected).

It is observed, that for a moderately large value of p, say $p \approx 1/2$, the system becomes unstable very fast, percolating the $S_k = +1$ state everywhere almost instantaneously.

However, as one decreases p, the system presents a well defined scenario. Fig. 8 shows the typical evolution of a percolation pattern in time. More precisely, the system nucleates bubbles of infected states ($S_k = +1$) and two scenarios are possible, either these bubbles continues to grow or they stop (compare Fig. 8 b & c). In analogy with the instability of a first order phase transition, it should exist a critical radius of nucleation that depends explicitly on p.

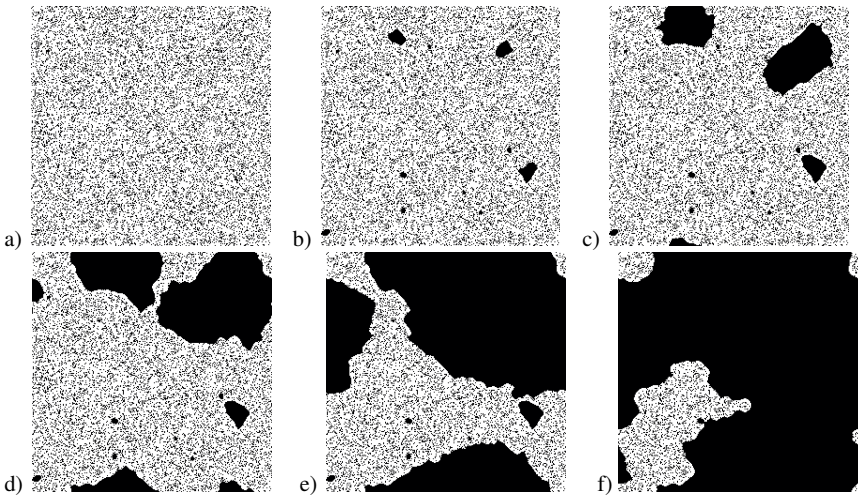

Fig. 8 Bootstrap percolation's patterns at six different time steps. The network is a square periodic lattice of $N = 256^2$ sites with a uniform vicinity of $|V| = 24$ sites. a) display the initial random state with an initial fraction 0.2 of $S_k = +1$ (that is, a given site is +1 with probability 0.2, and -1 with probability 0.8); In b) one observes the nucleation of bubbles, which eventually would propagate the +1 state over the random phase; In c) one observes that some infected bubbles have not reach the critical size and they do not propagate; however, in d) big bubbles invade the system transforming the interface in a front propagation over the whole system e) and f).

This critical radius of nucleation maybe estimated in the limit of large vicinity, in other words, in the range of validity of the mean field approximation. Let be p the fraction of infected sites initially distributed randomly in the system and a the radius of the vicinity ($\pi a^2 = |V|$). We shall add an infection bubble with a radius R (see Fig. 9-a). A $S_k = -1$ state in the boundary of the infected circle will become infected if $\sum_k S_k(t) = (2p-1)(\pi r^2 - A(R)) + A(R) > 0$, where $A(R)$ is the surface of the portion of the circle inside the infection bubble (see Fig. 9-b). Therefore, the bubble will infect neighbors and will propagate into the system, if

$$\frac{A(R)}{\pi a^2} > \frac{1-2p}{2(1-p)}. \tag{11}$$

The surface $A(R)$ follows from a direct geometrical calculation. In the large R/a limit, one gets

$$\frac{A(R)}{\pi a^2} \approx \frac{1}{2} - \frac{a}{3\pi R} + \mathcal{O}(R^{-3}),$$

therefore, one concludes that the critical radius of nucleation scales as

$$\frac{R_c}{a} \approx \frac{2(1-p)}{3\pi p}.$$

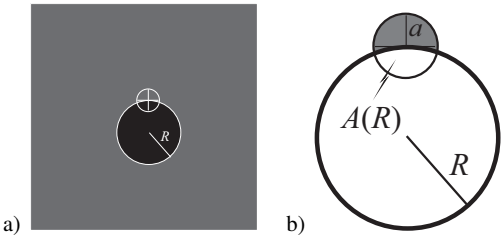

Fig. 9 a) Scheme for the mean field estimation of the critical radius of infection. The gray region represents the random initial data with a fraction p of +1. b) Details of the geometry for the calculation of $A(R)$.

Figure 10 shows a numerical study of the nucleation radius, for various vicinity sizes, $|V|$, as a function of p. Moreover the figure also presents the mean field estimation by an explicit geometrical calculation of the surface $A(R)$ and using the critical condition (11). One sees that the mean field approach matches perfectly with the data in the large $|V|$ limit.

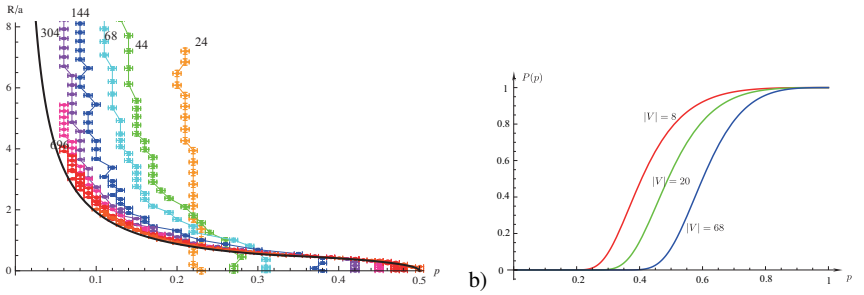

Fig. 10 a) Critical radius of nucleation R/a as a function of p. As expected as $p \to 1/2$ the critical radius is zero, while as $p \to 0$ the critical radius diverges. The points correspond to the numerical simulations for different values of the vicinity size: $|V| = \{24, 44, 68, 144, 304, 696\}$ as indicated in the figure. b) Estimation of the lower bound of the probability $P(p)$ of having a critical nucleation bubble of infected states, for $|V| = 8$, $|V| = 20$ and $|V| = 68$ One notices that this probability takes-off around a precise value of p.

However, a question remains open: what is the probability to obtain, *ab-initio* a bubble with a radius larger than R_c? This probability seems to be very small, because it is proportional to the probability to obtain πR_c^2 sates +1 all together, that is

$$P_{\text{bubble}} \approx p^{\pi R_c^2} = p^{|V|(R_c/a)^2} \sim p^{|V|\frac{4(1-p)^2}{9\pi^2 p^2}},$$

with R_c/a the function of p plotted in Fig. 10. Although, this probability $P(p)$ is quite small, it is a lower bound for the problem of Bootstrap percolation. If, initially, a bubble has a radius greater than $R_c(p)$, then the system percolates, and the nucleation bubble may not initially exist, but it may be built solely by the evolution, this provides a better estimation of the probability $P(p)$ of percolation.

4 Discussion

We have shown how different models amalgamate their underlying behavior under the common principle of the Ising-based models: Phase transitions, Bifurcations and Phase Diagrams and most important, the existence of a core principle, *e.g.*, energy minimization which appears to be a robust feature of these models and which would require a deeper consideration.

It is a remarkable fact, however, how despite a continued interest over the last century, the Ising model continues to fascinate and amaze us, not only on it's original context, but also in some other areas of knowledge were it has been applied. The "paramagnetic-ferromagnetic" transition can be recovered in all models described here, with deeper consequences, for example, in the field of human behavior, specially social sciences. Here we can ask ourselves for example: can the sudden changes of opinion before an election or the choice of a product or racial segregation be related to the basic physics of the Ising model?. Even more, the existence of an energy principle, something completely excluded and extraneous to the field of Social Sciences, seems to be the main thread behind, for studying and trying to understand human and social behavior. Certainly, delving deeper on this energy principle would require more attention and research. Finally we conclude by asking, Can we have some hope, in a near future and in the context of Social Science, of being able to develop predictive tools for studying and understanding better the human behavior ?

Acknowledgements The authors acknowledge Eric Goles, Pablo Medina, Iván Rapaport, and Enrique Tirapegui for their partial contribution to some aspects of the present paper, as well as Aldo Marcareño, Andrea Repetto, Gonzalo Ruz and Romualdo Tabensky for fruitful discussions and valuable comments on different topics of this work. This work is supported by Núcleo Milenio Modelos de Crisis NS130017 CONICYT (Chile). FU. also thanks CONICYT-Chile under the Doctoral scholarship 21140319.

References

1. Lenz, W., Physikalische Zeitschrift **21**, 613–615 (1920)
2. Ising, E., Beitrag zur Theorie des Ferromagnetismus, Zeitschrift für Physik **31**, 253–258 (1925)
3. Brush, S.G., History of the Lenz-Ising Model Rev. Mod. Phys. **39**, 883 (1967)
4. Glauber, R.J.: Time-Dependent Statistics of the Ising Model", J. Math. Phys. **4**, 294–307 (1963), doi: 10.1063/1.1703954
5. Brock, W.A., Durlauf, S.N., A formal model of theory choice in science, Economic Theory **14**, 113–130 (1999).
6. Brock, W.A., Durlauf, S.N., Interactions-Based Models, Handbook of Econometrics, **5**, Edited by J.J. Heckman and E. Leader, Chapter 54, p 3297–3380 (2001)
7. Bouchaud, J-P., Crises and Collective Socio-Economic Phenomena: Simple Models and Challenges, J. of Stat.Phys. **151**, 567–606 (2013)
8. Vichniac, G.: Simulating Physics with Cellular Automata, Physica, **D 10**, 96–116 (1984)
9. Pomeau, Y.: Invariant in cellular automata, J. Phys. A: Math. Gen., **17** L415–L418 (1984)

10. Goles, E., Rica, S.: Irreversibility and spontaneous appearance of coherent behavior in reversible systems, Eur. Phys. J. , **D 62**, 127–137 (2011)
11. Onsager, L.: Crystal Statistics. I. A Two-Dimensional Model with an Order-Disorder Transition, Phys. Rev. **65**, 117–149 (1944)
12. Yang, C.N.:The Spontaneous Magnetization of a Two-Dimensional Ising Model, Phys. Rev. **85**, 808–816 (1952)
13. Felipe Urbina, Sergio Rica and Enrique Tirapegui, "Coarse-Graining and Master equation in a Reversible and Conservative System", Discontinuity, Nonlinearity, and Complexity **4** (2) 199?208, (2015).
14. Schelling, T.C. : Models of Segregation, American Economic Review **59**, 488–493, (1969)
15. Schelling, T.C.: Dynamic Models of Segregation, Journal of Mathematical Sociology **1**, 143–186, (1971)
16. Schelling, T.C.: Micromotives and macrobehavior, New York, W.W. Norton (2006)
17. N. Goles Domic, E. Goles & S. Rica, "Dynamics and Complexity of the Schelling segregation model", Phys. Rev. **E 83**, 056111 (2011).
18. J. Chalupa, P.L. Leath, G.R. Reich, Bootstrap percolation on a Bethe lattice, J. Phys. C, Solid State Phys. **12** L31–L35 (1979)
19. Stauffer, D., Solomon, S., Ising, Schelling and Self-Organising Segregation, Eur. Phys. J. **B 57**, 473 (2007)
20. Singh, A., Vainchtein, D., Weiss, H. : Schelling's Segregation Model: Parameters, scaling, and aggregation, **21**, 341–366 (2009)
21. Gauvin, L., Vannimenus, J, Nadal, J.-P., Eur. Phys. J. **B 70**, 293 (2009)
22. V. Cortez, P. Medina, E. Goles, R. Zarama, & S. Rica, Attractors, statistics and fluctuations of the dynamics of the Schelling's model for social segregation, Eur. Phys. J. B **88**: 25 (2015).
23. J. Balogh, B. Bollobás, R. Morris, Majority bootstrap percolation on the hypercube, Comb. Probab. Comput. **18**, 17–51 (2009)
24. J. Balogh, B. Pittel, Bootstrap percolation on the random regular graph, Random Struct. Algorithms **30** 257–286 (2007)